Ceramics International 44 (2018) 12174–12179

Contents lists available at ScienceDirect

Ceramics International

journal homepage: www.elsevier.com/locate/ceramint

Synthesis of ZnO rod arrays on aluminum recyclable paper and effect of the rod size on power density of eco-friendly nanogenerators

Saionara V. Costa, Nilsa T. Azana, Pei Shieh, Talita Mazon*

Centro de Tecnologia da Informação Renato Archer, CTI, Rod. D.Pedro I, KM 143.6, CEP 13069-901 Campinas, SP, Brazil

ARTICLE INFO

Keywords:
Triboelectric nanogenerator
ZnO
Aluminum recyclable paper

ABSTRACT

In this work, we demonstrated a novel and effective approach on the use of low-cost electrodes, an eco-friendly substrate and zinc oxide (ZnO) micro or nanorods (MRs or NRs, respectively) for building triboelectric devices (TENGs). The reported strategy focuses on using low-cost materials and fabrication processes. For the first time and without any pre-treatment, an aluminum recyclable paper from the milk carton (named ARP) was used as a substrate and TENG bottom electrode. A systematic study on the growing of ZnO structures on ARP by chemical bath deposition has been carried out. We found that the ZnO rods size, and resistivity of the TENG upper electrode considerably influence the power density of the device. Such sustainable, low-priced ZnO-based TENGs can produce up to 1.6μW/cm^2 output power density when operated at 50 Hz. The fabrication of an eco-friendly nanogenerator demonstrates the possibility of manufacturing low-cost, flexible, and large-area energy harvesting devices for future applications.

1. Introduction

In the last years, researchers have started looking for new devices able to harvest different kinds of wasted mechanical energies from the environment and effectively convert such energies into electricity [1,2]. In this scenario, nanogenerators have emerged as a promising technology to produce electric power enough to drive some small functional devices, like light-emitting diodes (LEDs) and sensors, at low costs [3–6].

Among the existing types of nanogenerators for this purpose, the piezoelectric (PENGs) and triboelectric (TENGs) ones are those that have been receiving increased attention in the last decade [3–10]. In PENGs, the deformation of nanostructures by mechanical energy causes negative and positive charge separation generating an electric current [6,8–10]. In TENGs, on the other hand, the charges are generated by triboelectric effect (viz. contact and induction electrification) when two different materials are brought in contact and rubbed [2–5,7]. Briefly, during the contact in the triboelectric effect, each material develops a charge of opposite polarity [4]. The magnitude and polarity of the generated static charges are sensitivity to material composition, contact surface and the environmental [11].

TENGs show the advantage of providing high-output energy density with simple structures and easier packaging. Moreover, TENGs afford the possibility of using a variety of materials [7] for their fabrication, including flexible and transparent substrates [4,5]. Although TENGs have been intensively studied, issues related to the energy loss occurring during the power-generation process still need to be overcome for more effective applications. In this context, ZnO nanostructures stand out as an excellent material to be used in TENGs inasmuch as they may increase the device surface area and improve the performance by reducing the energy loss [6].

ZnO is a wide band-gap (3.37 eV) semiconductor compound with excellent charge carrier transport properties and high crystalline quality [12,13]. ZnO nanostructures show high piezoelectric and pyroelectric coefficients and large electromechanical coupling [6]. The piezoelectricity in ZnO nanostructures (e.g., nanowires, nanorods) comes from the lack of a center of symmetry in wurtzite structure. In addition to such excellent electrical properties, ZnO nanostructures with distinctive morphologies are relatively easy to grow on different substrates, including flexible ones, by using low temperature and low-cost methodologies [14].

One of such interesting routes is the low-temperature ZnO synthesis in aqueous solution, a pioneer the Vayssieres publication [14]. This method has no restriction in respect to the kind of substrate employed, as long as it is not completely water-soluble. This opens up lots of possibilities for using low-cost flexible substrates to grow ZnO nanostrucutres, for exempla paper – the cheapest and most abundant existing flexible substrate [7]. The synthesis of ZnO on paper substrates and bacterial cellulose substrates with no need of surface modification has been successfully reported by us in a previous work [15].

* Corresponding author.
E-mail address: talita.mazon@cti.gov.br (T. Mazon).

https://doi.org/10.1016/j.ceramint.2018.03.272
Received 22 February 2018; Received in revised form 29 March 2018; Accepted 30 March 2018
Available online 31 March 2018

Flexible, lightweight triboelectric devices are particularly interesting for applications for powering portable electronics through low power consumption. From previous works, a wide variety of flexible substrates have been tested for this purpose, which include the use of Kapton, PET (polyethylene terephthalate) [9,16], PVC(polyvinyl chloride), PET/ITO (indium-tin oxide) [4], and PDMS (polydimethylsiloxane) [17]. However, these substrates are costly in comparison with paper, so the development of low-price device becomes compromised. Aiming to overcome this issue, the use of packaging cardboard as a substrate for solar cells toward self-sustainable intelligent packaging was reported recently as a proof-of-concept [18]. Nevertheless, one of the limitations in this case was the evaporation of aluminum (Al) contact an e-beam system, which does not contribute to a cost-effective device fabrication process.

To tackle the issue of developing a more affordable electronics, we demonstrate a cost-effective route to manufacture flexible, lightweight large-area nanogenerators based on ARP.

In this work, aluminum recyclable paper (ARP), readily obtained from a milk carton, with no need of additional surface treatments was used as the substrate and bottom electrode of ZnO-based TENGS. The device development involved the establishment of the ideal conditions for growing ZnO nanostructures on ARP, as our first target. Second, we used the ZnO micro and nanorods (here, namely MRs and NRs, respectively) to build TENGs devices as a proof-of-concept. We also tested different materials for the device upper electrode, such as copper foil or platinum/PTE. The evaluation of such experimental conditions is important as the size of ZnO rods and the characteristics of the upper electrodethe govern on the response of the triboelectric device.

2. Experimental

2.1. Materials

The aluminum recyclable paper (ARP) was obtained from a regular milk carton package (tetrapak®). Zinc acetate dihydrate 98%, Zn $(Ac)_2{\cdot}2H_2O$, Zinc nitrate hexahydrate 98%, $Zn(NO_3)_2{\cdot}6H_2O$, hexamethylenetetramine (HMTA) 99% were purchased from Sigma-Aldrich. An ethanolic solution (Ethanol absolute from Sigma Aldrich 98%) of zinc acetate dehydrate (Sigma-Aldrich) was used to prepare the nucleation layer by spray deposition.

Copper foil (Cu) was purchased from 3 M (Metal 1181 6035–11), and the platinum (Pt) film on PET was deposited by sputtering. The deposition of the 100 nm Pt film on PET substrate (Sigma Aldrich®) was performed in a Balzers (BA510) DC sputtering system in the LNNano Microfabrication Laboratory. The Pt film was deposited under a pressure of 2×10^{-7}mbar and at room temperature. The Pt film thickness was monitored by a quartz crystal microbalance sensor in the deposition chamber. The resistivity of the Pt/PET and Cu was measured by using Thin Film Devices, Inc. FPP-2000, presenting values of 5.3 Ohm.sq^{-1} and 0.005 Ohm. sq^{-1}, respectively.

2.2. Growth of ZnO nanostructures on ARP

ZnO micro and nanostructures were synthesized directly on the ARP substrate without any surface treatments on the carton. Chemical bath deposition (CDB) synthesis was used for growing ZnO rods. The details for the ZnO structures growth on ARP are discussed in the following.

2.3. Preparation of the ARP substrate

ARP mainly consists of three layers: paperboard, an Al layer and a polyethylene film (PE) (Fig. 1a). Thus, to use the aluminum layer as the bottom electrode, it is required to remove the polyethylene film. The polyethylene film was mechanically peel off using tweezers (Fig. 1b), preserving the Al layer underneath. After that, ARP substrate was rinsed with acetone to eliminate any residual polymer adhered to the surface. Following, ARP substrate was immersed in a 1 mol L^{-1} sodium hydroxide (NaOH) solution for three minutes to promote hydrophilic characteristics to the surface and, consequently, better wetting of the zinc acetate ethanolic.

2.4. Seeding layer deposition by ultrasonic spray

A seeding layer based on zinc acetate ethanolic solution was deposited on ARP by ultrasonic spray coating method. An *ExactaCoat Ultrasonic Coating System - Sono-Tek microspray* (Fig. S1), and a 10 mM zinc acetate $Zn(Ac)_2$ ethanolic solution was used during deposition. Table S1 shows a summary of the parameters of deposition used here.

2.5. Synthesis of ZnO micro and nanostructures on ARP substrate

ZnO micro and nanostructures were grown over the seeded ARP by chemical bath deposition (CBD). $Zn(NO_3)_2{\cdot}6H_2O$ and HMTA were mixed in a 10 mM equimolar aqueous solution [15]. The reagents and the substrate were put in a Teflon cup and the CBD process was carried out in neutral pH at 95 °C for 2 h (Fig. S2). To complete the process, the substrates were withdrawn from the solution, rinsed with deionized water and dried in air at 90 °C using a hot plate.

2.6. Characterization

The surfaces of the bare ARP and ZnO coated substrates were characterized by scanning electron microscope (SEM), energy dispersive X-ray spectroscopy (EDS), X-ray diffraction (XRD), and atomic force microscopy (AFM). The SEM images and EDS were obtained through an Inspect F50- SEM from FEI by using 5 kV and 12 μA. The XRD results were obtained by using a Shimadzu-XDR 7000 diffractometer with a copper tube CuKα (α = 1.54060 Å), a graphite monochromator, and operated at a power of 40 kV and 30 mA. Nanosurf AFM was used to image the surface topography in the non-contact/phase contrast mode. A surface profiler (Dektak 150) was used to measure the thickness of the layer.

The resistivity of the Al layer on the ARP was obtained by using the four points method and a Keithley 4200-SCS equipment.

To test the triboelectric devices, we employed a special structure designed and built as described by Shieh et al. [19]. In the Test System, the sinusoidal signals are supplied by Wavetek Datron model 29 A signal generator. The signal is amplified by a Sonata Sonasom AM/FM stereo audio amplifier. The device response is monitored by a Taktronix TDS2014B oscilloscope that provides the voltage supplied by the device. The audio amplifier provides vibration on the Test System allowing the device strikes against a planar surface and bending due to its flexibility. The device compression against a planar surface enables the contact and separation of charges on the electrode surface. All triboelectric devices were built with a contact surface area of 4.4 × 4.4 cm, using the configuration showed in Fig. 1.e. All TENGs measurements were driven with a load of 10 MΩ. The TENGs were tested in different frequencies to find out the maximum electrical response.

3. Results and discussion

3.1. Characterization of the ARP substrate

From SEM and AFM characterization, the ARP substrate exhibited a homogeneous surface with apparently low roughness (Fig. 1c and d). EDS confirms the presence of Al on the card. XRD analysis shows well-defined peaks corresponding to the Al structure (Fig. S3.a and Fig. S3.b, respectively (111), (200), (311)).

Additional AFM analyses provided roughness values (root-mean-square, R_{ms}) of the 115.3 nm and 615 nm for scanned areas having 3 × 3 μm^2 and 10 × 10 μm^2, respectively (Fig. 1d and Fig. S3c).

The electrical measurements on the ARP surface show an average

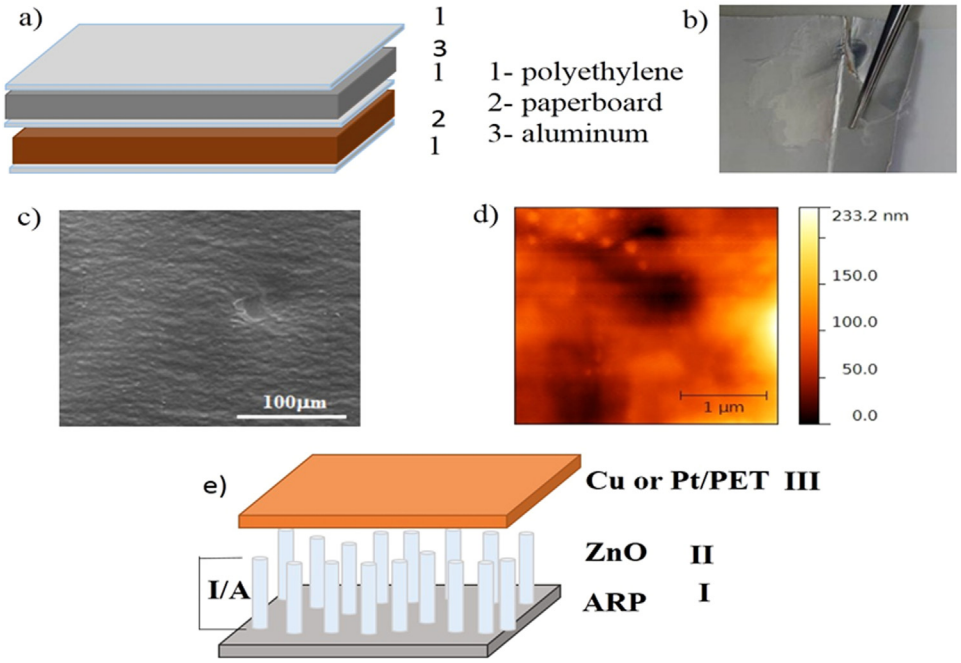

Fig. 1. a) Structure of aluminum recyclable paper (ARP) substrate - tetrapak®. b) Picture shows the partially removing of the polyethylene film. c) SEM image of the ARP surface after film be withdrawn. d) AFM topographic image of the ARP surface after film be pulled off. e) Schematic structure of triboelectric nanogenerator: I) ARP as bottom electrode and substrate, II) ZnO structures grown by chemical bath deposition, III) Copper tape or Platinum/PET as upper electrode.

sheet resistance (R_{sheet}) of approximately 57 mΩ , after removing of the polyethylene film. The thickness of the aluminum film is 60 µm (0.006 cm), measured with a digital micrometer. Thus, using Eq. (1), the resistivity (ρ) of the ARP was 3.42 × 10^{-4} Ω cm, a value similar to those typically exhibited by transparent conductor oxide (TCO) substrate. This indicates that the aluminum layer of the ARP substrate can be used as a bottom electrode in TENGs.

$$\rho = \boldsymbol{Rsheet} \times \textbf{thickness} \quad (1)$$

3.2. Characterization of ZnO micro and nanostructures on ARP

Before growing ZnO structures onto ARP, a seed layer based on zinc acetate ethanolic solution was previously deposited. As well known, the seed layer is the key for growing high-quality ZnO nanorods. The thickness of the seed layer and the number of Zn^{2+} ions are significant parameters to be controlled once they determine the size and density of ZnO rods [20,21].

SEM images, Fig. 2, show the influence of the number of seed layers on the growth of ZnO micro or nanorods. The deposition of 10 layers promotes the growth of a mix of ZnO micro- (MRs) and nanorods (NRs) onto ARP surface (Fig. 2.a). That means, thinner layers and lower Zn^{2+} sites, lead to the growth of the nano and microstructures with a large distribution in diameter, from 0.5 to 1.2 µm (Fig. S4.a). Conversely, the deposition of 20 seed layers favors the growth of homogeneously distributed ZnO NRs onto ARP, with hexagonal base and diameter around 80–110 nm (Fig. 2.b and Fig. S4.b). As it commented above, the thickness of the ZnAc film and the number of Zn^{2+} sites are parameters that need to be considered for growing homogeneous ZnO nanorods onto ARP.

The effectiveness of covering a 4.4 × 4.4 cm ARP area with ZnO MRs or NRs is clearly shown in Fig. 2.c. The novelty reported herein is a meaningful step towards the growing ZnO nanostructures on ARP, opening new possibilities for the development of low-cost and disposable devices.

Fig. 2.d shows the XRD spectra obtained after growing ZnO (either NRs or MRs) over ARP substrate. It is possible to verify well-defined peaks corresponding to the hexagonal structure of ZnO, according to JCPDS 36-1451. The presence of these peaks corroborates the efficient route for growing ZnO over ARP substrate by CDB.

In an attempt to obtain the thickness of ZnO films, the FEG-SEM images were performed in the film cross section, as depicted in Fig. S5. The thickness of the Al layer is around 5 µm and of the ZnO nanostructures layer is around 6–8 µm.

3.3. Triboelectric nanogenerator – proof-of-concept

A special structure was designed and built to test triboelectric nanogenerators as a proof-of-concept device. The test system is composed by different modules for generating vibration signals, for checking mechanical movement and measuring the electrical response.

Electrical power generated by triboelectric materials hinges on the vibration characteristics, dielectric material and size of the device. Each triboelectric device has a frequency where the maximum response is obtained. In our test system, the vibration allows the contact and separation of the surfaces, pressing the device against a planar surface. At the same time, the vibration allows the device bending, due to its inherent flexibility.

Fig. 3 illustrates the working mechanism of the contact-separation mode for triboelectric nanogenerators. When the original state is submitted an external pressure, the two layers are brought into contact. As a result, tribo- and inductive charges are generated and distributed on contact surfaces. By releasing the pressure, it occurs a separation of two materials and a final current flow from the Al ARP to the upper electrode through the external load. After that, the nanogenerator achieves the electrical equilibrium.

The peak-to-peak (Pk-Pk) output voltage, measured at 40 and 50 Hz, are shown in Fig. 4, with the operational parameters for all test devices described in Table 1. Although all measurements were only driven by 10 MΩ load, it is possible to state that our devices work as TENGs. Here, the best response was achieved at 40 Hz for the device using ZnO NRs and Pt/PET upper electrode. For other device architectures, 50 Hz was the ideal operational frequency.

From Fig. 4, one can conclude that the morphology and size of the ZnO rods (i.e. MRs or NRs), as well as, the resistivity and malleability of the upper electrode influence the performance of the disposable TENGs. The devices built from a mix of ZnO MRs and NRs show lower power density than those using only ZnO NRs, as shown in Table 1. The best performance of ZnO NRs can be attributed to their higher surface area. The use of ZnO NRs increases the effective contact area, as well as the

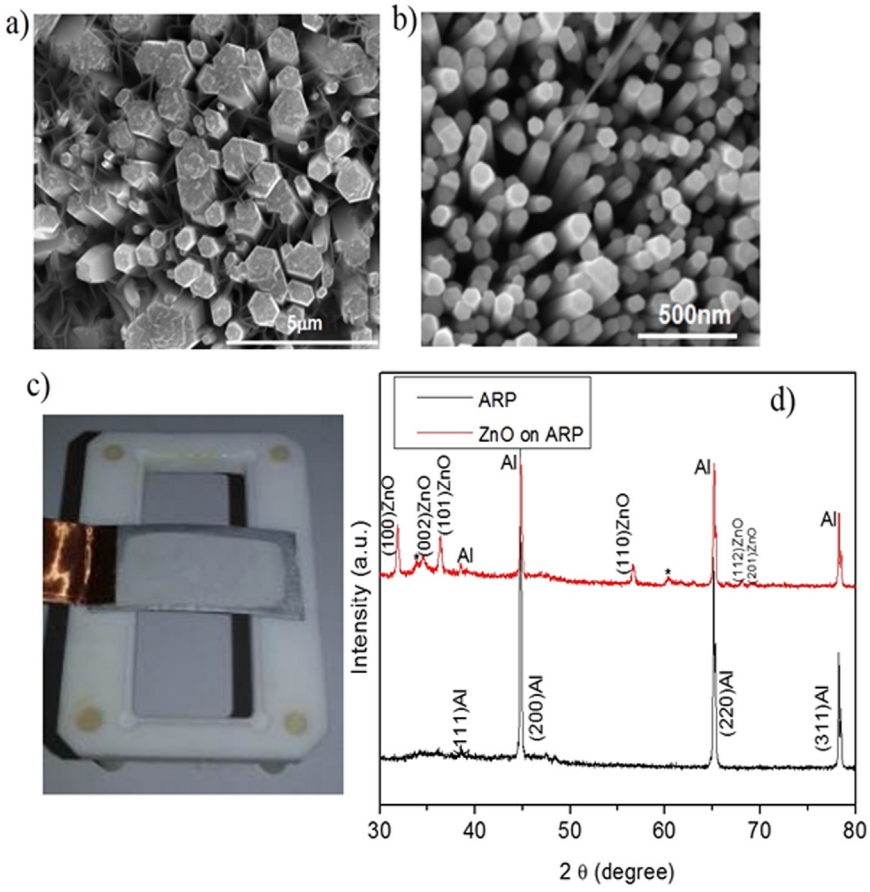

Fig. 2. FEG-SEM images of the ZnO micro and nanorods surface grown onto ARP. The nucleation layer was prepared with 10 mM of concentration in ethanol. a) 10 layers and b) 20 layers deposited by ultrasonic spray followed of ZnO grow by CBD with equimolar concentration 10 mM of $ZnNO_3$:HMTA at 95 °C/2 h. c) Picture of ZnO homogeneous rods grown on ARP.d) XRD patters of: a)black is just ARP substrate, aluminum side.b) red is ARP substrate with ZnO nanorods grown by CBD by using 20 layers of nucleation.

contact electrification charges [20]. Additionally, the ZnO MRs are harder to deform, leading to a worse performance compared with the NRs-based devices. The smaller surface area of the ZnO MRs compromises the contact electrification charges and, therefore, the power density.

We also observed that higher power densities are obtained by using Cu tape than Pt/PET as the upper electrode. One of the reasons is the high malleability of the Cu tape, that enlarges the effective contact area by the strong interaction with the nanorods. The other is the lower resistivity of the Cu tape (0.005 Ωsq^{-1}), in comparison with the Pt/PET electrode (5.3 Ωsq^{-1}). This contributes to higher currents from the ARP to Cu tape electrode through the external load. It is well known that in TENGs the output performance is determined by the choices of two different materials that will be in contact [22–24]. In literature, metals,

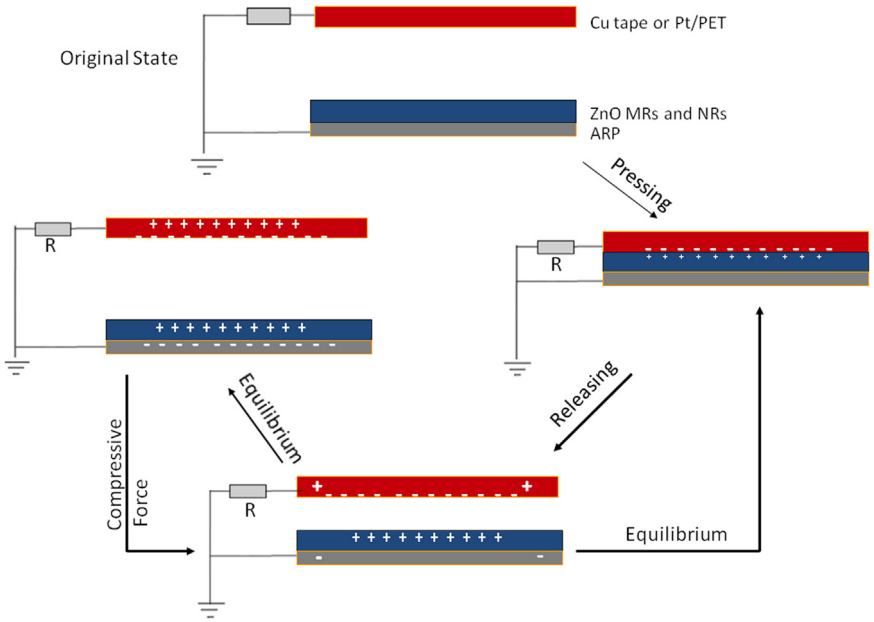

Fig. 3. Working mechanism of triboelectric nanogenerator on ARP.

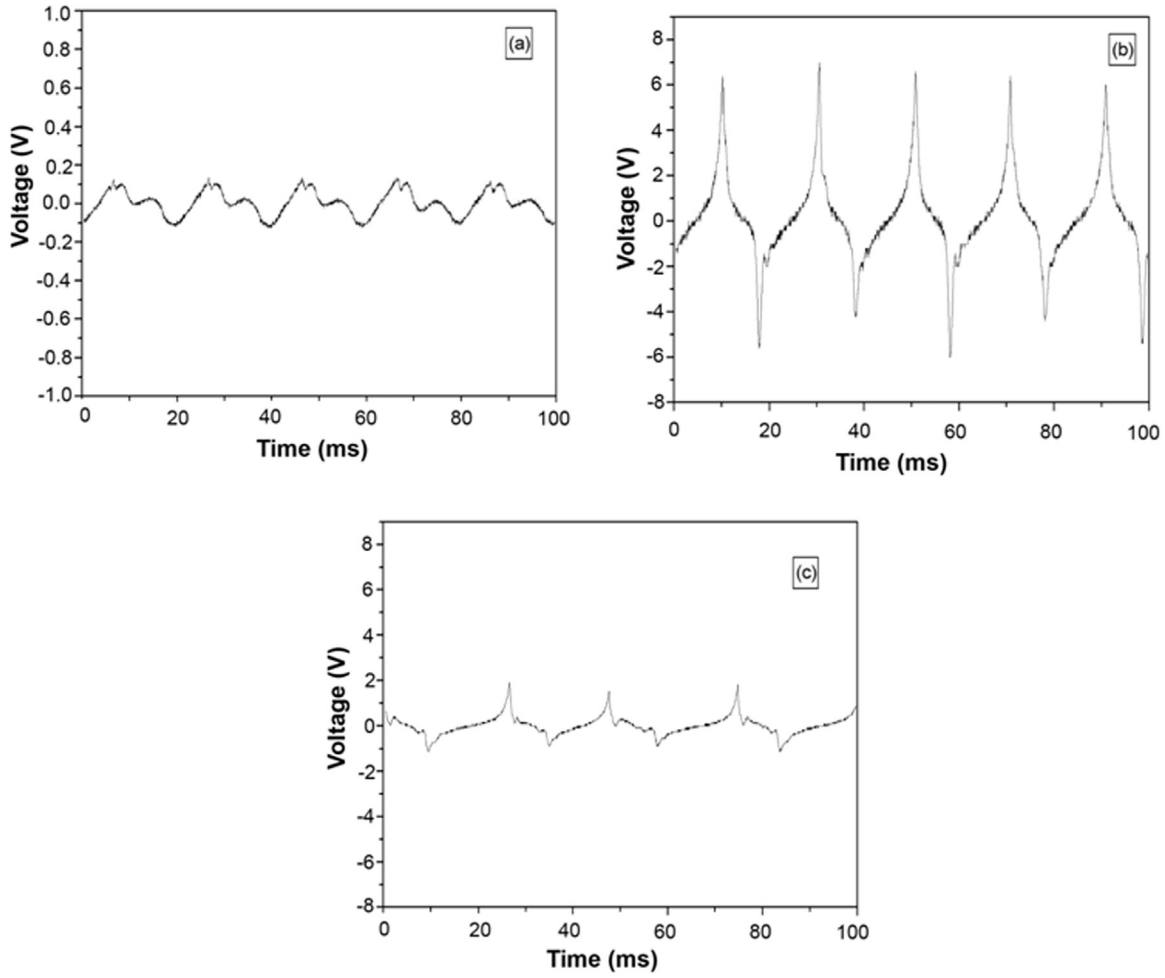

Fig. 4. Peak-to-peak (Pk-Pk) output voltage measurements: a) at 50 Hz of nanogenerators prepared with a mix ZnO MRs and NRs with Cu tape as upper electrode, b) at 50 Hz of nanogenerators prepared with ZnO NRs with Cu tape as upper electrode, and c) at 40 Hz of nanogenerators prepared with ZnO NRs with Pt/PET as upper electrode.

oxides, polymers and organic materials have been arranged on the triboelectric series, according to their ability to gain or lose electrons. [22–27] The higher positioned materials will acquire a positive charge when contacted with a material from the bottom of the series, and the charge transfer will be more effective the farther one material from the other is positioned in the series. In the triboelectric series, the Pt is farther from ZnO than the Cu (Fig. S6). Our power density results obtained demonstrated that, besides of Triboelectric Series; the electrical and mechanical properties of the electrodes must be also considered when building TENGs devices.

Here, the best power density found was 1.6μW/cm^2 for TENGS-based on ZnO NRs and Cu tape as upper electrode, Table 1. Although previous reports [19] show TENGs –based on ZnO NRs with power densities of up to 70 mW/m^2, the load used in our work is much lower (10 MΩ in comparison with 250 MΩ from the literature). [19,20] The lower value of load may have contributed to lesser power density. However, the great differential of this work relies on the possibility of building nanogenerators by using a cheap, eco-friendly recyclable material as both the bottom electrode and substrate. To the best our knowledge, this is also the first demonstration of a low-cost and disposable TENG. This kind of device may open up the path for feeding sensors in several new applications, especially in controlling the quality of food during transportation.

4. Conclusions

In summary, we presented an eco-friendly, large-area, flexible and cheap triboelectric nanogenerator (TENG) with good performance based on ZnO nanostructures and recyclable paper (ARP). The fabrication processes of ZnO, both micro and nanostructures, and packaging of the TENGs are low-cost, scalable, and compatible with various other substrates. A systematic study was conducted to correlate ZnO rods size, and upper electrode properties with TENG performance. The best performance, 1.6 μW/cm^2 and 179 nA, was obtained for TENGs employing a Cu upper electrode and ZnO NRs on ARP bottom electrode, when driven by 10 MΩ load.

Table 1
Electrical measurements of the TENGs with a mix of ZnO MRs and NRs or ZnO NRs using different types of upper electrodes.

Morphology	Upper electrode	V_{pp} (mV)	V_{rms} (mV)	Power (nW)	Current (nA)	Power Density (nW/cm^2)
MRs and NRs	Cu tape	272	16	0.03	1.6	0.13
NRs	Cu tape	11800	1790	320	179	1655.01
NRs	Pt/PET	3120	828	69	82.8	354.12

The devices here showed good performance and reproducibility and open up the path for using a recyclable substrate and low-temperature process toward sustainable electronics.

Acknowledgements

The authors would like to be thankful to CNPq (577526/2008-1) and the Center for Research and Development of Functional Materials CEPID - FAPESP (2013/07296-2) Brazilian Agencies by the financial support and the LME/LNNano - Brazilian Nanotechnology National Laboratory/CNPEM/MCTI by the support in SEM images. We also thank Rafael Furlan de Oliveira for revising the English language of the manuscript.

Supplementary information

The following files are available free of charge.

Picture of the spray used in seed layer step - Spray *ExactaCoat Ultrasonic Coating System - Sono-Tek microspray®,* parameters of seeding layer deposition by ultrasonic spray coating method, picture of the chemical bath deposition system used to growth ZnO structures, micro and nanorods. EDS, XRD and AFM of the aluminum recyclable paper surface. Distribution of sample diameters: a) ZnO microrods b) ZnO nanorods. FEG-SEM cross section image of the aluminum recyclable paper: around 5 μm thickness of the aluminum layer and 6–8 μm thickness of the ZnO micro and nanostructures.

Appendix A. Supporting information

Supplementary data associated with this article can be found in the online version at http://dx.doi.org/10.1016/j.ceramint.2018.03.272.

References

[1] International energy agency. World Energy Outlook 〈http://www.iea.org/publications/freepublications/publication/WorldEnergyOutlook2016ExecutiveSummaryEnglish.pdf〉 (Accessed 16 January 2016).
[2] F.R. Fan, Z.Q. Tian, Z. Lin Wang, Flexible triboelectric generator, Nano Energy 1 (2012) 328–334.
[3] S. Wang, L. Lin, Z.L. Wang, Nanoscale-triboelectric-effect enabled energy conversion for sustainable powering of portable electronics, Nano Lett. 12 (2012) 6339–6346.
[4] F.-R. Fan, J. Luo, W. Tang, C. Li, C. Zhang, Z. Tian, Z.L. Wang, Highly transparent and flexible triboelectric nanogenerators: performance improvements and fundamental mechanisms, J. Mater. Chem. A 2 (2014) 13219–13225.
[5] F. Fan, L. Lin, G. Zhu, W. Wu, R. Zhang, Z.L. Wang, Transparent triboelectric nanogenerators and self-powered pressure sensors based on micropatterned plastic films, Nano Lett. 12 (2012) 3109–3114.
[6] Z.L. Wang, J. Song, Piezoelectric nanogenerators based on zinc oxide nanowire arrays, Science 312 (2006) 242–246.
[7] Y. Zi, L. Lin, J. Wang, S. Wang, J. Chen, X. Fan, P.K. Yang, F. Yi, Z.L. Wang, Triboelectric-pyroelectric-piezoelectric hybrid cell for high-efficiency energy-harvesting and self-powered sensing, Adv. Mater. 27 (2015) 2340–2347.
[8] C.C. Jin, X.C. Liu, H.H. Fan, Y. Wang, H.L. Hwang, Y.F. Zhang, Q. Wang, Fabrication and structure of lead-free BCTZ-MWCNTs composite and its application in energy harvesting, Ceram. Int. 43 (2017) 15886–15890.
[9] K.-S. Choa, D.-H. Kima, Y.-H. Kimb, J. Nahb, H.-K. Kim, Li-doped Cu_2O/ZnO heterojunction for flexible and semi-transparent piezoelectric nanogenerators, Ceram. Int. 43 (2017) 2279–2287.
[10] Y.F. Kou, Z.M. Kou, D.P. Zhao, Z.J. Wang, G.J. Gao, X.J. Chai, Fabrication of lead-free $Ba(Zr_{0.2}Ti_{0.8})O$-3-$(Ba_{0.7}Ca_{0.3})TiO_3$ nanoparticles and the application in flexible piezoelectric nanogenerator, Ceram. Int. 43 (2017) 4803–4806.
[11] R.D.I.G. Dharmasena, K.D.G.I. Jayawardena, C.A. Mills, J.H.B. Deane, J.V. Anguita, R.A. Dorey, S.R.P. Silva, Triboelectric nanogenerators: providing a fundamental framework, Energy Environ. Sci. 10 (2017) 1801–18011.
[12] Z.L. Wang, Zinc oxide nanostructures: growth, properties and applications, J. Phys.-Condens. Matter 16 (2004) R829–R858.
[13] L.-Y. Chen, Y.-T. Yin, Efficient electron transport in ZnO nanowire/nanoparticle dye-sensitized solar cells via continuous flow injection process, RSC Adv. 3 (2013) 8480–8488.
[14] B.L. Vayssieres, Growth of arrayed nanorods and nanowires of ZnO from aqueous solutions, Adv. Mater. 5 (2003) 464–466.
[15] S.V. Costa, A.S. Gonçalves, M.A. Zaguete, T. Mazon, A.F. Nogueira, ZnO nanostructures directly grown on paper and bacterial cellulose substrates without any surface modification layer, Chem. Commun. 49 (2013) 8096–8098.
[16] B.N. Chandrashekar, B. Deng, A.S. Smitha, Y. Chen, C. Tan, H. Zhang, H. Peng, Z. Liu, Roll-to-roll green transfer of CVD graphene onto plastic for a transparent and flexible triboelectric nanogenerator, Adv. Mater. 27 (2015) 5210–5216.
[17] X. Yue, Y. Xi, C. Hu, X. He, S. Dai, L. Cheng, G. Wang, Enhanced output-power of nanogenerator by modifying PDMS film with lateral ZnO nanotubes and Ag nanowires, RSC Adv. 5 (2015) 32566–32571.
[18] A. Vicente, H. Águas, T. Mateus, A. Araújo, A. Lyubchyk, S. Siitonen, E. Fortunato, R. Martins, Solar cells for self-sustainable intelligent packaging, J. Mater. Chem. A 3 (2015) 13226–13236.
[19] P.J. Shieh, N.T. Azana, T.E.A. Santos, A.V. Martins, N.L. Dias, A.L. Xavier, Methodology for choosing piezoelectric devices using piezoelectric energy harvesting to feed massive use of RFID tags (No. September), 2014 IEEE Bras. RFID (2014) 46–49.
[20] X. Yang, W.A. Daoud, Triboelectric and piezoelectric effects in a combined tribo-piezoelectric nanogenerator based on an interfacial zno nanostructure, Adv. Funct. Mater. 26 (2016) 8194–8201.
[21] E. Pourshaban, H. Abdizadeh, M.R. Golobostanfard, A close correlation between nucleation sites, growth and final properties of ZnO nanorod arrays: sol-gel assisted chemical bath deposition process, Ceram. Int. 42 (2016) 14721–14729.
[22] S.-H. Shin, Y.E. Bae, H.K. Moon, J. Kim, S.-H. Choi, Y. Kim, H.J. Yoon, M.H. Lee, J. Nah, Formation of triboelectric series via atomic-level surface functionalization for triboelectric energy harvesting, ACS Nano 11 (2017) 6131–6138.
[23] K.-E. Byun, Y. Cho, M. Seol, S. Kim, S.-W. Kim, H.-J. Shin, S. Park, S. Hwang, Control of triboelectrification by engineering surface dipole and surface electronic state, ACS Appl. Mater. Interface 8 (2016) 18519–18525.
[24] A.F. Diaz, R.M. Felix-Navarro, A semi-quantitative tribo-electric series for polymeric materials: the influence of chemical structure and properties, J. Electrost. 62 (2004) 277–290.
[25] X. Zhang, X. Huang, S.W. Kwok, S. Soh, Designing non-charging surfaces from non-conductive polymers, Adv. Mater. 28 (2016) 3024–3029.
[26] S. Niu, Z.L. Wang, Theoretical systems of triboelectric nanogenerators, Nano Energy 14 (2015) 161–192.
[27] Y.J. Kim, J. Lee, S. Park, C. Park, C. Park, H.-J. Choi, Effect of the relative permittivity of oxides on the performance of triboelectric nanogenerators, RCS Adv. 78 (2017) 49368–49373.